A unified model for subaqueous bedform dynamics

Douglas J. Jerolmack[1] and David Mohrig[2]

Department of Earth, Atmospheric and Planetary Sciences, Massachusetts Institute of Technology, Cambridge, Massachusetts 02139, USA

1. E-mail: **douglasj@mit.edu**; Phone: 617-253-1949 (Corresponding author).

2. E-mail: **mohrig@mit.edu**; Phone: 617-253-9429.

In Press, Water Resources Research

Abstract. Bedform evolution remains dynamic even in the special case of steady, uniform flow. Data from the sandy, braided North Loup River, Nebraska, USA, show that roughness features on the channel bottom display a statistical steady-state and robust scaling that are maintained through the collective interactions of transient (short-lived) bedforms. Motivated by such field data, and laboratory observations of bedform growth, we develop a nonlinear stochastic surface evolution model for the topography of bedload-dominated sandy rivers in which instantaneous sediment flux explicitly depends on local elevation and slope. This model quantitatively reproduces laboratory observations of initial growth and saturation of bedforms from a flat surface, and also generates long-term dynamical behavior characteristic of natural systems. We argue that the variability in geometry and kinematics of bedforms in steady flow, and the existence of roughness at all wavelengths up to the largest dunes, are a consequence of the nonlinear relationship between sediment flux and topography, subject to noise.

1. INTRODUCTION

The nonlinear dependence of sediment transport on surface topography produces a bewildering array of patterns, from ripples at the centimeter scale to river networks and depositional fans at a basin scale. A natural way to characterize such patterns involves measuring static geometrical properties, spatial correlations, and scaling laws that may be exhibited between physical parameters of the system [e.g., *Rubin*, 1992; *Dodds and Rothman*, 2000]. Landscapes are dynamic (i.e. variable in time), however the study of their transient behavior is hindered by the slow rate of evolution of most geological systems. Although surface evolution equations are naturally time-dependent, the

dynamical predictions of erosional landscape models [see, e.g., *Willgoose et al.*, 1991**;** *Howard*, 1994] are difficult to test. A geomorphological transport system that exhibits both transient behavior on observable time scales and statistically-robust geometrical properties allows strong tests of models, and provides a window into fundamental pattern formation mechanisms in sedimentary systems. Trains of bedforms in sand-bedded rivers are one example of such a system.

While bedform classification schemes, such as distinguishing ripples from dunes [e.g., *Ashley*, 1990], may be useful in describing some aspects of bedform behavior, they belie the continuum of scales of topography that make up a sand-bedded channel. Indeed, there is theoretical [*Hino*, 1968], laboratory [*Hino*, 1968; *Nordin*, 1971] and field evidence [*Levey et al.*, 1980; *Nikora et al.*, 1997] that roughness of all wavelengths exists below the scale of the largest dunes. Further, bedforms in natural systems change dimensions continuously as they migrate downstream. The internal dynamics of a train of bedforms manifests itself as variability in bedform height, length and migration rate (celerity), and in bedform deformation, even when the topography is developing under steady and uniform macroscopic flow conditions [*van den Berg*, 1987; *Gabel*, 1993; *Mohrig*, 1994; *Leclair*, 2002]. Although great progress has been made in the understanding of instability and bedform growth from a flat surface [e.g., *Smith*, 1970; *McLean*, 1990], current models cannot describe the long-time behavior of a train of finite-amplitude bedforms.

Increasingly sophisticated measurements of the flow field over rigid topography [e.g., *Nelson et al.*, 1993; *McLean et al.*, 1994; *Maddux et al.*, 2003a,b] have demonstrated the influence of topography on turbulence production and bed stress. There

is now little doubt that the most accurate model of bedform evolution will eventually come from detailed numerical solution of the Navier-Stokes equations [e.g., *Shimizu et al.*, 2000], coupled to some force balance on sand grains and sediment continuity. Currently, however, the modeling of fluid flow over arbitrary (and rapidly deforming) topography is a formidable challenge. Moreover, a fully-coupled fluid-sediment-topography model would be sufficiently complex that it could not easily serve as an exploratory tool for understanding fundamental aspects of sand bed evolution.

At present, an incomplete understanding of how irregular bed topography controls turbulence production and how this turbulence affects local sediment transport precludes development of a bedform evolution model from first principles. Several models have been proposed that are fundamentally discrete and stochastic, with sediment transport represented by simple rules [e.g., *Tufillaro*, 1993; *Werner*, 1995; *Niño et al.*, 2002]. Self-organization of bedforms in such models is robust, and in some cases many different bedform shapes may be reproduced by variation of coefficients or transport rules [*Werner*, 1995]. While these models have been effective in illustrating how microscopic disorder can create macroscopic order [see *Tufillaro*, 1993], their abstract nature prevents quantitative comparison to natural systems. Sediment transport in such models is essentially represented as stochastically-driven directed diffusion. A family of deterministic continuum models for eolian ripple formation has been proposed by physicists based on phenomenological descriptions [e.g., *Terzidis et al.*, 1998; *Prigozhin*, 1999; *Valance and Rioual*, 1999] or conservation and symmetry principles [e.g., *Csahók et al.*, 2000], but these approaches do not allow the interpretation of coefficients in terms of measurable physical quantities [see *Csahók et al.*, 1999]. Many more models for eolian

ripples have been proposed in the literature, with similar behavior, limitations and caveats to those described above.

In bedload-dominated systems, it is well established that topography exerts a first-order control on sediment flux. In particular, *Gomez et al.* [1989] have linked instantaneous sediment flux, q_s, directly to the passage of bedforms, showing that the majority of variance in q_s may be explained by topography. *Gomez and Phillips* [1999] found that the highest frequency variations in q_s, however, cannot be related directly to the passage of bedforms, and interpreted them as representing high-dimensional chaos (deterministic uncertainty) in the transport system. Motivated by these findings, and by documented time evolution of bedforms in the North Loup River, Nebraska, USA, we develop a model including both a deterministic surface evolution equation based on parameterization of bed stress in terms of local topography and stochastic fluctuations in sediment flux. In this paper we focus on qualitative behavior not captured in the previously mentioned models for bedform evolution, and perform a preliminary analysis of temporal and spatial scaling with comparisons to empirical data. In a future work we will report more quantitative comparisons to field data.

2. RIVER DATA

We present here topographic data capturing bedform evolution in time and in space that are derived from low altitude aerial photography of the braided North Loup River, Nebraska, USA [*Mohrig*, 1994; *Mohrig and Smith*, 1996], which has a bed consisting of well-sorted medium sand (Trask sorting coefficient = 1.32; median grain diameter, d_{50} = 0.31 mm). Time-lapse images taken with a camera suspended beneath a tethered helium-

filled balloon were converted into topographic maps (Fig. 1a), where the grayscale pixel intensity was transformed into water depth using the Beer-Lambert Law [*Soo*, 1999] calibrated to numerous surveyed points within the channel. The spatial (downstream and cross-stream, or x- and y-direction, respectively) resolution is known to be 0.02 m from image pixel size, while we estimate vertical resolution to be ~0.01 m from analysis of sequential bedform profiles. Observations shown here were taken with an interval of one minute for a period of one hour, covering a section of the river of 30 m x 15 m. Approximately constant river stage ensured that flow was essentially steady over the observation period, so the observed variability and adjustments of bedform geometry and migration rate were caused by internal dynamics of the sediment-fluid interface. A complete statistical description of channel-bottom topography, and the method developed to measure this topography, will be the focus of a later paper. Here we present salient properties of bed evolution in the North Loup River that we believe are representative of sand-bedded rivers in general, and these observations serve to motivate the development of a new mathematical description for the dynamics of bedforms in bedload-dominated sandy rivers.

It is convenient to examine elevation along one dimension (i.e. 1D profiles in the downstream direction) to observe changes in cross-sectional geometry, and our data show that all downstream profiles at a given snapshot in time are statistically identical (as determined by scaling methods presented below) and therefore justify a 1D analysis. Sequential profiles stacked in time (Fig. 1b) show that bedforms are not translation-invariant. While large-scale bed features remain recognizable over the duration of observation (40 minutes), individual bedforms are observed to split into smaller features,

merge to form larger features, spontaneously form on the stoss side of larger features, and disappear in the lee slope of larger features. We see then that bedforms are inherently transient objects, such that the river bottom remains dynamic even in steady flow. Individual bedforms become unrecognizable after migrating one to two wavelengths, similar to observations of sand dunes in rivers in Eastern Europe by *Nikora et al.* [1997] and laboratory dunes observed by *Leclair* [2002].

Rather than subjectively identify and define individual bedforms from a profile, the series of elevations in a profile is treated as a random function [see *Nikora et al.*, 1997], and its variability is characterized as roughness. A simple and common measure of roughness is the root mean square of elevation on the interface, sometimes referred to as the interface width, w [*Barabási and Stanley*, 1995]:

$$w = \left[\frac{1}{N} \sum_{i=1}^{N} (\eta_i - \bar{\eta})^2 \right]^{1/2}, \qquad (1)$$

where N is the number of observations, η is bed elevation and the over-bar represents an average over the domain considered. For reference, the average bedform height for a profile from the North Loup River is about two times the measured value of w for that profile.

The scaling of w with observed length or "window size", l, contains information about the size distribution of roughness elements, and is often found to exhibit a power law over some range for rough interfaces:

$$w \sim l^{\alpha}, \qquad (2)$$

where α is the roughness exponent, characterizing the scaling of elevation fluctuations [see *Barabási and Stanley*, 1995; *Dodds and Rothman*, 2000]. For North Loup River profiles, we determine w for every box of the smallest window size, which is twice the data resolution or 0.04 m. We then take the average of all w values to obtain a characteristic roughness for that window size. This procedure is repeated for sequentially larger window sizes, up to one-half the size of the observation domain (~15 m); a similar analysis was performed by *Nikora and Hicks* [1997]. An example result is shown in figure 2, which plots the characteristic interface width against window size for downstream profiles at a snapshot in time. There are several features worthy of note. First, there is a scale-invariant regime in which a power-law relationship holds between w and l, where the slope of the line in the scaling regime is the roughness exponent. Second, there is a gradual roll over of the interface width with window size at the transition between the lower scaling regime and the upper saturation regime. This transition occurs at a length equal to the characteristic wavelength of the largest dunes; the associated transition length and interface width values are l_x and w_x, respectively (Fig. 2). Repeating this analysis of w for profiles taken at different times but at the same location yields the same values for α, l_x and w_x, suggesting the scaling of roughness elements is stationary. Taken together, these results show that despite the transience of individual topographic elements, the river-bottom maintains a statistical steady-state in terms of roughness.

The river-bed displays a continuum of scales of topography up to the wavelength of the largest features, as represented by the power-law relationship between w and l, and no clear distinction can be made between ripples and dunes. A similar conclusion is reached by computing the power spectra of bed profiles (not shown), which contains equivalent information about roughness scaling. These results are not unique to the North Loup River; similar findings have been reported in the laboratory [*Hino*, 1968; *Nordin*, 1971] and field [*Levey et al.*, 1980; *Nikora et al.*, 1997], and may be the rule in sand-bedded systems, rather than the exception. The two regimes present in figure 2, power-law roughness growth and saturation, may be indicative of different organizing physical processes. In many interface problems such as crystal growth, the scale invariant regime is generated by internal dynamics of the interface itself, while saturation occurs due to 'finite size effects', where growth is limited by the size of the container [see *Barabási and Stanley*, 1995]. In the case of bedforms, scale invariance may be due to the local sediment transport physics, while maximum dune size is controlled by boundary conditions such as water depth or background shear stress.

Qualitatively, the existence of many scales of topography may be understood from examining the temporal evolution of topography in successive profiles (Fig. 1c). The largest dune features translate by the motion of smaller bedforms on their backs. These smaller features spontaneously form on a dune back, then grow in amplitude as they migrate across the dune back before disappearing in the subsequent trough [as discussed by *Jain and Kennedy*, 1974; *Nikora et al.*, 1997; *Gomez and Phillips*, 1999]. The appearance, growth and disappearance of bedforms maintains a constant distribution of

channel roughness, and this process is a fundamental organizing principle that should be reproduced by a model of sand-bed evolution.

3. MODEL DEVELOPMENT

We seek an intuitive, physically realistic, continuum model capable of reproducing both the instability of a flat sand bed subjected to a shear flow, and the long-time evolution of dynamic topography. We focus on bedforms built from a uni-modal distribution of particle sizes moving primarily as bedload because this sediment flux can be treated as responding instantaneously to changes in the flow field without accruing significant error. We hypothesize that the detailed structure of the fluid flow field is not important for determining temporal and spatial scaling, and hence we can write a "local growth model" [*Barabási and Stanley*, 1995; *Dodds and Rothman*, 2000] for the evolution of the sediment-fluid interface – this hypothesis is tested below. This said, the three main ingredients to our model are (i) a relationship between sediment flux and local bed elevation; (ii) the dependence of sediment flux on local flow strength (here characterized by bed shear stress, τ); and (iii) the dependence of flow strength on local topography. The first model condition is simply a statement of mass conservation:

$$\frac{\partial \eta}{\partial t} = -\frac{1}{(1-p)}\frac{\partial q_s}{\partial x}, \tag{3}$$

where t is time, p is porosity and q_s is sediment flux with dimensions L^2/T. The second condition takes the form of a power-law relationship between sediment flux and boundary shear stress:

$$q_s = m\tau^{n}, \tag{4}$$

where n is generally 1.5 [*Meyer-Peter and Müller*, 1948] but may vary up to 2.5 [*Fernandez-Luque and van Beek*, 1976] and m can vary between 5.7 and 12 depending on the rate of sediment transport (Wiberg and Smith, 1989). Equation 4 could also be written in terms of an excess stress above that value required for initiation of grain motion; our intent here, however, is simply to write down the most generic representation of the governing equations.

Our third model condition relates the local boundary shear stress to the local bed topography. Specifically it relates shear stress to bed elevation and bed slope as

$$\tau(x) = \tau_b\left(1 + A\frac{\eta}{\langle h\rangle} + B\frac{\partial\eta}{\partial x}\right), \tag{5}$$

where ‹h› is the spatially-averaged depth of flow at the beginning of a run, τ_b is the background boundary shear stress associated with ‹h›, η is vertical distance of a point on the local sediment-fluid interface from the mean elevation, and A and B are coefficients (Fig. 3). This equation for stress in terms of local topography may be considered a Taylor expansion, where higher-order spatial derivatives have been neglected. Relating local bed stress to local bed elevation was first proposed by *Exner* [1925] who noted that conservation of fluid mass required an increase in the vertically-averaged velocity over the top of an arbitrary two-dimensional bump and derived an explicit relationship between bed

stress and topography by relating bed stress to the square of vertically-averaged fluid velocity. Neglecting higher order terms (i.e., $\eta/\langle h \rangle << 1$) *Exner* [1925] found that:

$$\tau(x) = \tau_b \left(1 + 2\frac{\eta}{\langle h \rangle} \right). \quad (6)$$

Smith [1970] and *Engelund* [1970] were the first to propose that the magnitude of local shear stress is also a function of the local bed slope. *Smith* [1970] argued that the relationship between local bed slope and local bed stress is a consequence of the fluid inertia. Moving water is not easily deflected and as a result, steep adverse slopes put relatively high velocity fluid closer to the bed, producing larger values of bed stress [see also *Nelson et al.*, 1993]. Equation 5 simply sums the contributions of relative bed elevation (6) and slope to arrive at a value for bed stress at every site on the bed. The predicted variation of bed stress over topography using (5) is consistent with measured bed stress over static dunes in the laboratory [*Nelson et al.,* 1993; *McLean et al.*, 1994].

3.1. One-dimensional surface evolution equation

3.1.1. Exner's equation

Combining equations 3, 4 and 6 gives the result:

$$\frac{\partial \eta}{\partial t} = -\langle q_s \rangle \frac{2n}{\langle h \rangle (1-p)} \left(1 + 2\frac{\eta}{\langle h \rangle} \right)^{n-1} \frac{\partial \eta}{\partial x}, \quad (7)$$

a nonlinear wave equation describing surface evolution. The explicit dependence of advection on bed elevation means that points of higher elevation move faster. *Exner* [1925] used (7) to explain why bedforms become skewed with downstream transport [see *Smith*, 1970]. An angle-of-repose condition must be added to this equation to stop the lee surfaces of bedforms from oversteepening unrealistically. The nonlinear wave equation (7) is neutrally stable, i.e. perturbations neither grow nor decay in amplitude with time. While this lack of instability renders (7) inadequate as a general bedform-evolution model, (7) serves as a useful point of departure for our elaboration described next.

3.1.2. New surface evolution equation

Equations 3, 4 and 5 represent our complete model system in one dimension. Combining them, we arrive at a new surface evolution equation for sand-bedded channels:

$$\frac{\partial \eta}{\partial t} = -\langle q_s \rangle \frac{n}{(1-p)} \left(\frac{A}{\langle h \rangle} \frac{\partial \eta}{\partial x} + B \frac{\partial^2 \eta}{\partial x^2} \right) \left(1 + A \frac{\eta}{\langle h \rangle} + B \frac{\partial \eta}{\partial x} \right)^{n-1} . \qquad (8)$$

The simple addition of a slope-dependent contribution to bed stress produces a surface evolution equation that is quite different from Exner's equation (7). Equation 8 contains not only a nonlinear advection term, but also a nonlinear diffusion term. The diffusion term may change sign in this formulation, and negative diffusion leads to the growth of perturbations on the surface.

A formal stability analysis of (8) is beyond the scope of this paper and here we only provide a qualitative discussion of the bed instability following *Smith* [1970] and *McLean* [1990]. From (3) we may write:

$$\frac{\partial \eta}{\partial t} = -\frac{1}{(1-p)}\frac{\partial q_s}{\partial \tau}\frac{\partial \tau}{\partial x}. \qquad (9)$$

Since $\partial q_s/\partial\tau$ is always positive it is the shear stress gradient that determines the sign of $\partial\eta/\partial t$, and hence whether the bed undergoes erosion or deposition. Because sediment deposition occurs downstream of the stress maximum a perturbation on the stream bed may cause another bump to grow downstream of it, ultimately leading to a train of finite-amplitude bedforms. When elevation is small the stress maximum is upstream from the crest of a bump, causing the bump to continue growing. As elevation becomes large, the stress maximum shifts to the elevation maximum and deposition no longer occurs on the crest – growth ceases.

3.1.3. Stochastic form

High-frequency fluctuations in sediment flux are a direct consequence of turbulence-aided sediment transport [*Nelson et al.*, 1995; *Gomez and Phillips*, 1999; *Schmeeckle and Nelson*, 2003; *Sumer et al*., 2003]. While fluctuations in instantaneous bed stress may be modeled deterministically in a fluid-mechanical model, we treat this variability as stochastic and explore its morphodynamic importance by addition of a noise term. The stochastic surface evolution equation then reads:

$$\frac{\partial \eta}{\partial t} = -\langle q_s \rangle \frac{n}{(1-p)}\left(\frac{A}{\langle h \rangle}\frac{\partial \eta}{\partial x} + B\frac{\partial^2 \eta}{\partial x^2}\right)\left(1 + A\frac{\eta}{\langle h \rangle} + B\frac{\partial \eta}{\partial x}\right)^{n-1} + \zeta(x,t), \qquad (10)$$

where $\zeta(x, t)$ is Gaussian-distributed low-amplitude white noise, although the time evolution of (10) turns out to be insensitive to the details of $\zeta(x, t)$. A stochastic partial differential equation like (10) can produce long-range spatial correlations on the interface even when the term describing interface growth or transport is entirely local in origin [*Rubin*, 1992; *Barabási and Stanley*, 1995].

3.2. Two-dimensional surface evolution equation

Our surface-evolution equation can be made two-dimensional through inclusion of a lateral diffusion term. The principle transport direction is still downstream, while lateral sediment transport has a magnitude dependent on the cross-stream (y-direction) slope [*Murray and Paola*, 1997; *Hersen*, 2004]. In essence, sediment flux is calculated as one-dimensional downstream slices which are coupled to neighboring slices via the lateral diffusion of sediment. A deterministic form of the two-dimensional model then consists of (8) plus a lateral diffusion term

$$\frac{\partial \eta}{\partial t} = -\langle q_s \rangle \frac{n}{(1-p)} \left(\frac{A}{\langle h \rangle} \frac{\partial \eta}{\partial x} + B \frac{\partial^2 \eta}{\partial x^2} \right) \left(1 + A \frac{\eta}{\langle h \rangle} + B \frac{\partial \eta}{\partial x} \right)^{n-1} + D \frac{\partial^2 \eta}{\partial y^2}, \qquad (11)$$

where D is the lateral diffusivity constant (units L^2/T). Note that this treatment of lateral sediment transport is identical to equation 10 in *Hersen* [2004] and similar to the explicit slope-dependent transport used in *Murray and Paola* [1997]. This approach makes the assumption that the fundamental transport mechanisms occur in the downstream direction, and that cross-stream sediment flux depends linearly on slope; it is the simplest formulation consistent with observation [e.g., *Parker*, 1984]. A stochastic form of the two-dimensional model simply consists of (11) plus a noise term,

$$\frac{\partial \eta}{\partial t} = -\langle q_s \rangle \frac{n}{(1-p)} \left(\frac{A}{\langle h \rangle} \frac{\partial \eta}{\partial x} + B \frac{\partial^2 \eta}{\partial x^2} \right) \left(1 + A \frac{\eta}{\langle h \rangle} + B \frac{\partial \eta}{\partial x} \right)^{n-1} + D \frac{\partial^2 \eta}{\partial y^2} + \zeta(x, y, t) . \quad (12)$$

Equation 12 is our new anisotropic "local growth equation" for depositional systems. We expect the applicability of (12) to be general, but it may be made specific by calibration of coefficients to a particular situation. In order to realistically simulate the morphodynamics of a train of subaqueous bedforms, several additional ingredients are required for numerical implementation and are discussed next.

3.3. Numerical method

We explore the dynamical behavior of our model system by solving discrete versions of eqs. (3), (4) and (5) at every location on the 2D grid, where *i* and *j* represent the *x* and *y* grid positions, respectively. Boundary conditions used are periodic in the downstream direction and zero flux in the cross-stream direction. Grid size is 100 x 50 cells. Larger domain sizes were explored, but did not have any significant effect on model results. The initial condition for model runs is a flat, horizontal surface seeded with elevation perturbations of very low amplitude produced as white noise. Values for grid spacing Δx (equal in *x* and *y* directions), time step Δt, water depth $\langle h \rangle$, all coefficients and background shear stress, τ_b, are specified at the beginning of a model run; the exponent n = 1.5 for all simulations. At a given time step, the following sequence of operations is performed:

$$\tau_{i,j} = \tau_b \left(1 + A \frac{\eta_{i,j}}{\langle h \rangle} + B \frac{\eta_{i,j} - \eta_{i-1,j}}{\Delta x} \right), \quad (13)$$

$$\tau_{i,j} = \begin{cases} \tau_{i,j}; \geq 0 \\ 0; < 0 \end{cases}, \tag{14}$$

$$q_{a_{i,j}} = \begin{cases} E\left[\left(\frac{\eta_{i,j} - \eta_{i+1,j}}{\Delta x}\right)^2 - (\tan\theta_c)^2\right]\left(\frac{\eta_{i,j} - \eta_{i+1,j}}{\Delta x}\right); \left(\frac{\eta_{i,j} - \eta_{i+1,j}}{\Delta x}\right) > \tan\theta_c \\ 0; \left(\frac{\eta_{i,j} - \eta_{i+1,j}}{\Delta x}\right) \leq \tan\theta_c \end{cases}, \tag{15}$$

$$q_{s_{i,j}} = m\tau_{i,j}{}^{n} + q_{a_{i,j}} + \zeta_{i,j}, \tag{16}$$

$$\Delta\eta_{i,j} = -\frac{\Delta t}{(1-p)\Delta x}\left(q_{s_{i,j}} - q_{s_{i-1,j}}\right) + \frac{\Delta t D}{(\Delta x)^2}\left(\eta_{i+1,j} + \eta_{i-1,j} + \eta_{i,j+1} + \eta_{i,j-1} - 4\eta_{i,j}\right). \tag{17}$$

Equation 13 computes bed stress using an upwind scheme for slope, and (14) makes all negative bed stresses zero, crudely mimicking the shadow zone of low transport occurring immediately downstream from a bedform lee face. In order to prevent oversteepening of lee surfaces we employ a version of the grain-avalanching proxy as presented by *Hersen* [2004]. If the downwind-calculated slope exceeds the critical angle, θ_c, then an additional 'avalanche flux' is computed using (15). If the chosen value for coefficient *E* is sufficiently large, any slope that builds to an angle > θ_c relaxes instantaneously at the next time step. Equation 16 determines the sediment flux at each grid point by summing the contributions from local bed stress, avalanching and noise; the noise term is zero for deterministic model runs. Finally, (17) finds elevation change using a 1D, upwind version of the sediment continuity equation. The second term on the right hand side of (17) is a diffusion term, solved by calculating the discrete 2D laplacian of the elevation field, and scaled using a diffusivity *D* which represents the importance of lateral coupling of sediment transport. Although the explicit diffusion term in (12) is for the *y*-direction only, in our numerical implementation (17) we add an explicit 2D diffusive term which serves

the additional purpose of numerical dissipation [*Press et al.*, 1988], helping to smooth the elevation field to enhance numerical stability.

The choice of coefficients for bed stress and sediment transport relations is presently unconstrained. In practice, A and B could be estimated empirically from laboratory observations of bed stress over topography, while cross-stream sediment transport could be treated in a more rigorous manner using an explicit method such as *Parker* [1984]. Values for m may be selected from the literature. Varying coefficients affects the growth rate and amplitude of bed features, but does not greatly affect temporal or spatial scaling. Here we are interested in whether the general equations 13-17 can produce a variety of dynamical behavior observed in laboratory and field settings, so coefficients were selected such that the contributions of elevation and slope to the total bed stress are approximately equal, and cross-stream sediment transport is a small fraction of the downstream flux – see table 1. We will perform future experiments to estimate these coefficients. Grid spacing and time step values were selected from considerations of numerical stability and computation time.

4. RESULTS

4.1. Deterministic model ($\zeta = 0$)

Numerically solving (13)-(17) with appropriately chosen coefficients (table 1) reproduces growth and saturation of bedforms from a perturbed flat surface, and evolving bedforms display nonuniform geometries characteristic of natural topography (Fig. 4). Additionally, celerity is roughly inversely related to bedform height, and merging of

bedforms occurs due to varying migration speeds [as in experiments by *Coleman and Melville*, 1994] in a manner similar to models of eolian ripple development [*Caps and Vandewalle*, 2001; *Prigozhin*, 1999; *Schwämmle and Herrmann*, 2004]. In contrast to these previous eolian models where the coarsening of bedforms continues until there is only one bedform in the model domain, the steady-state solution of our model consists of a train of bedforms. Steady state for model output is verified by computing α, w_x and l_x at several different times to ensure there is no systematic drift.

Cross-stream diffusion provides sufficient coupling to generate sinuous-crested bedforms whose width occupies the entire model domain (Fig. 4a). Crestline terminations, or defects, are observed to migrate through the system faster than the bedforms, as postulated by *Werner and Kocurek* [1997], and seen in previous numerical simulations [*Caps and Vandewalle*, 2001; *Yizhaq et al.*, 2004]. In contrast to *Werner and Kocurek* [1999; see also *Werner*, 1999] who treat bedform crestlines and defects as independent dynamical variables, crestlines and defects in our model arise naturally from the local coupling of sediment transport to topography, and so are a consequence rather than a cause of the dynamics. In the deterministic scenario, $\zeta = 0$ for $t > 0$, nonuniform transient evolution occurs because of the spatial noise inherited from initial conditions. At long time, the bedforms evolve toward uniform, straight-crested features. In other words, the final state of the deterministic model is a static state (in a lagrangian frame), with only one scale of topography.

The growth of bed roughness with time can be quantified by calculating the interface width of downstream profiles over the entire model domain for each time step using (1). To facilitate comparison to previous data, interface width and model time are

scaled by their respective equilibrium values, or the values corresponding to saturation of roughness growth. Several authors [e.g., *Baas*, 1994; *Niño et al.*, 2002] have found experimentally that bedform growth is fit well by an exponential function of the form

$$\frac{w}{w_{eq}} = 1 - e^{-\gamma \frac{t}{t_{eq}}}, \tag{18}$$

where $\gamma = 6$ provides a good fit to most data [see also *Nikora and Hicks*, 1997] and the subscript *eq* denotes equilibrium values. Equation 18 with $\gamma = 6$ provides an excellent fit to the growth of bed roughness for the deterministic model (Fig. 5a), implying the essential dynamics of bedform development are captured in the model. In another set of experiments reported by *Nikora and Hicks* [1997], a power law relationship was observed:

$$\frac{w}{w_{eq}} = \begin{cases} \left(\frac{t}{t_{eq}} \right)^{\beta}; t < t_{eq} \\ 1; t \geq t_{eq} \end{cases}, \tag{19}$$

where β, the growth exponent [as in *Barabási and Stanley*, 1995], was found to be 0.28 under the laboratory conditions examined. This power law relation does not fit the deterministic model data, a topic we return to below**.**

The general model behavior is not very sensitive to changes in values of the coefficients. The bedform instability is present if *B* is positive, and sinuous-crested

bedforms develop as long as there is a weak lateral coupling via diffusion. We verified numerically that spatial and temporal scaling are unaffected by varying coefficients – only growth rate and amplitude of bed features change.

4.2. Stochastic model

Addition of noise has a profound influence on bedform dynamics and spatial scaling. Low amplitude noise (run S – see table 1) produces growth of bed roughness from a flat surface that is well-fit by *Nikora and Hicks*' [1997] power-law relation (19), as seen in figure 5b. In other words, the presence of noise shifts the development of roughness from an exponential to a power law trajectory, and ultimately increases the saturation amplitude of bed features.

From a cursory glance it is apparent that bedforms of many scales co-exist on the fully developed model interface (Fig. 6) with 2D morphology that compares well to bedforms measured in the North Loup River (Fig. 1a). Stacked sequential profiles from the model at steady state show bedforms that are continuously varying in shape (Fig. 6b), with the emergence and disappearance of bedforms being an ongoing process. Perhaps the most notable aspect of the stochastic model results is their qualitative similarity to steady-state dynamics observed in the river data. Sequential profiles generated by the model clearly show larger dune-like topography mantled with smaller ripple-like topography that spontaneously emerges in the troughs of the larger forms and rapidly moves over their stoss sides (Fig. 6c). The ripple-like forms grow in amplitude as they migrate across the stoss sides of the larger bedforms, only to be absorbed by the lee faces of the larger forms. This disappearance of the smaller bedforms provides the mass that

causes the larger forms to migrate downstream. As observed for river dunes, modeled bedforms become unrecognizable after migrating one to two wavelengths downstream.

We compare the spatial roughness scaling of our noisy model to data from the North Loup River using eqs. (1) and (2), where w and l are normalized by their transition values w_x and l_x, respectively (Fig. 7). The roughness exponent for the model, computed over the scaling regime, is 0.56, in reasonable agreement with the North Loup River. More importantly, the form of the roughness scaling curve from the North Loup River is reproduced by our noisy model results (Fig. 7). In particular, the existence of a large dominant wavelength, and a continuum of scales below that wavelength, along with the long cross-over to saturation, are captured by the model.

5. DISCUSSION

The striking difference in dynamical behavior between deterministic and noisy simulations provides insight into the importance of transport fluctuations in determining bed roughness properties. To gain an understanding of the physical processes controlling temporal growth of roughness we compare sediment transport conditions of two experimental studies. Transport stage is defined as $T = \psi/\psi_c$, where $\psi = \tau_b /[(\rho_s - \rho_f)d_{50}g]$ is the dimensionless shear stress, ψ_c is the critical value for initiation of motion of grains, ρ_s and ρ_f are the sediment and fluid density, respectively, and g is acceleration due to gravity . The exponential growth of bed roughness corresponds to low transport stage, while power law growth occurs at high transport stage. *Niño et al*. [2002] conducted all experiments in the range $2 < T < 3.3$, and their bedform growth curves (see their figure 10) are close to the exponential relation (18).

Flume runs reported by *Nikora and Hicks* [1997] span the range $9 < T < 30$ and display the power-law growth described by (19). Larger T certainly corresponds to larger fluctuations in sediment flux from direct influences of turbulence on bedload transport, and from suspended sediment transport where fluctuations in fluid stress have a greater influence.

The match of deterministic and stochastic model runs to the empirical exponential and power law growth relations, respectively, implies that in some sense the equations are capturing the features of sediment transport relevant to bedform evolution. Exponential growth of roughness in time is generally predicted for linear instabilities, while power law growth is a generic process of noisy interfaces [*Barabási and Stanley*, 1995]. The effect of noise in our model is to induce more rapid bedform growth early on, such that large roughness amplitude is achieved rapidly and hence the nonlinearity governs growth. *Coleman et al.* [2005] fit power-law growth relations to data over a range $3.4 < T < 32.9$. In reality, there is likely a gradual transition between exponential and power-law growth such that the respective relations are two end members in a spectrum. Indeed, numerical experiments with very low amplitude noise (not shown here) exhibit roughness growth intermediate between exponential and power law.

At long time, deterministic simulations evolve toward a steady state of uniform, periodic, straight-crested bedforms, i.e. a static steady state. Once the sediment flux field is exactly in phase with topography, evolution stops and the cross-stream diffusion ensures that all lateral variability disappears. This final state is not representative of trains of dunes in natural rivers. The long-time evolution of stochastic model runs consists of a bed that is continuously varying, but in statistical steady state. The

mechanistic explanation for this phenomenon is that noise creates small perturbations on the stream-bed that allow the growth of instabilities from the governing equations. The growth of new bedforms is balanced by the disappearance of bedforms in the troughs of larger features. The bed remains continuously dynamic because the sediment flux can never be exactly in phase with topography, and hence nonuniform divergences in sediment flux force continuous adjustments of bedforms.

6. CONCLUSIONS

The model results obtained here are for a uniform sediment size on a freely deformable surface (i.e. no nonerodible areas exist on the bed). Pattern formation in this model is robust, as evidenced by the lack of sensitivity to model coefficients. Robustness of pattern formation implies that the details of fluid flow may not be important for a first-order description of the bed dynamics. In other words, the sediment-fluid interface has an internal dynamic that is independent of the details of the system, and allows for a geometric description of its evolution.

There is much to explore in the dynamics of our model system (13)-(17), and the analyses presented here are meant only to demonstrate the promise of this approach. A great advantage of the model is its flexibility, which will allow examination of unsteady flow and complex boundary conditions in order to address issues relevant to river management. The fluid enters into the problem only through a small, interpretable set of coefficients that may be related to measured quantities. Equations 13-17 represent a unified model for subaqueous bedform dynamics because they provide a description of bedform initiation, development and steady-state behavior. Further, bedforms of

different scales arise from the same fundamental transport processes. Variability in the geometry and kinematics of bedforms is a consequence of the deterministic relationship between sediment flux and topography, and noise.

Modeled bedforms are self-organized in the sense that large-scale features arise from a completely local description of bed evolution, i.e. bedforms are produced from interactions between adjacent grid points in the model. Measurements of fluid flow around static bedforms show that topography can generate long-range disturbances in the flow field, in the form of turbulence production and coherent flow structures [*Nelson et al.*, 1993; *McLean et al.*, 1994; *Best et al.*, 1997; *Maddux et al.*, 2004a,b]. While the flow structure undoubtedly influences sediment transport, nonlocal effects introduced by turbulent fluid flow may be of second-order importance in determining the large-scale structure of the stream-bed. At the very least, this modeling approach shows that a completely local, geometric description of topographic evolution can generate realistic bedform dynamics, and even quantitatively model bedform growth (Fig. 5) and spatial scaling (Fig. 7). The presence of uncorrelated noise is sufficient to induce a dynamic steady state comparable to natural rivers. These results suggest that the presence of turbulence is important in terms of a perturbation source, but the structure of turbulence may be less important in terms of transport [*Sumer et al*., 2003] and bedform dynamics. A systematic numerical exploration of the structure (distribution) of noise and its influence on model behavior is necessary to address this issue, but is beyond the scope of this paper. We have observed no effect on scaling when the stochastic term is changed from gaussian to uniformly-distributed white noise.

An improved understanding of bedform evolution is required to predict the stage-discharge relationship in sand-bedded rivers [e.g., *Allen*, 1973; *Levey at al.*, 1980], and also to interpret bedform geometry from preserved cross-beds in the stratigraphic record [*Jerolmack and Mohrig*, 2005]. Dunes and ripples determine the flow resistance in sandy channels because they are the principle roughness elements on the bed. The manner in which bedforms adjust in space and in time determines, to a large extent, the cross-sectional geometry of a channel, because bottom roughness adjusts much more rapidly than channel width. The model presented here can be used to explore the response of a channel bottom to changes in sediment transport conditions. In future work we will calibrate the model to field and laboratory data.

Acknowledgements. This project was motivated by discussions with the "Novel methods for modeling the surface evolution of geomorphic interfaces" Working Group, held in May, 2004 at MIT and sponsored by the National Center for Earth-surface Dynamics. We acknowledge supportive and constructive reviews by Chris Paola, Vladimir Nikora, Stephen Coleman and Jon Pelletier. In addition, Brad Murray, Brandon McElroy and Wes Watters provided very helpful and stimulating discussions. McElroy also made invaluable contributions to data analysis of the North Loup River. This work was supported by the STC Program of the National Science Foundation via the National Center for Earth-surface Dynamics under Agreement Number EAR-0120914.

References sited

Allen, J.R.L., Phase differences between bed configuration and flow in natural environments, and their geological relevance, *Sedimentology*, *20*, 323-329, 1973.

Ashley, G., Classification of large-scale subaqueous bedforms: A new look at an old problem, *J. Sed. Petr.*, *60*, 160-172, 1990.

Baas, J.H., A flume study on the development and equilibrium morphology of current ripples in very fine sand, *Sedimentology*, *41*, 185-209, 1994.

Barabási, A.-L., and H.E. Stanley, Fractal concepts in surface growth, *Cambridge Univ. Press*, Cambridge, UK, 366pp, 1995.

Best, J., S. Bennett, J. Bridge and M. Leeder, Turbulence modulation and particle velocities over flat sand beds at low transport rates, *J. Hydraul.. Eng., 123*, 1118-1129, 1997.

Caps, H., and N. Vandewalle, Ripple and kink dynamics, *Phys. Rev. E*, *64*, 041302, 2001.

Coleman, S.E., and B.W. Melville, Bed-form development, *J. Hydraul. Eng.*, *120*, 544-560, 1994.

Coleman, S.E., and B.W. Melville, Initiation of bed forms on a flat sand bed, *J. Hydraul. Eng.*, *122*, 301-310, 1996.

Coleman, S.E., M.H. Zhang, and T.M. Clunie, Sediment-wave development in subcritical water flow*, J. Hydraul. Eng.*, *131*, 106-111, 2005.

Csahók, Z., C. Misbah, F. Rioual, and A. Valance, A class of nonlinear front evolution equations derived from geometry and conservation, *Physica D*, *128*, 87-100, 1999.

Csahók, Z., C. Misbah, F. Rioual, and A. Valance, Dynamics of aeolian sand ripples, *Euro. Phys. J. E*, *3*, 71-86, 2000.

Dodds, P.S., and D.H. Rothman, Scaling, Universality and Geomorphology, *Ann. Rev. Earth Planet. Sci.*, *28*, 571-610, 2000.

Engelund, F., Instability of erodible beds, *J. Fluid. Mech., 42*, 225-244, 1970.

Exner, F.M., Uber die Wechselwirkung zwischen Wasser und Geschiebe in Flüssen, *Sitzungsbericht Akad. Wiss. Wien*, *Abt. IIa 134*, 166-204, 1925 (in German).

Fernandez-Luque, R., and R. van Beek, Erosion and transport of bed-load sediment, *J. Hydraul Res.*, *14*, 127-144, 1976.

Gabel, S.L., Geometry and kinematics of dunes during steady and unsteady flows in the Calamus River, Nebraska, USA, *Sedimentology, 40*, 237-269, 1993.

Gomez, B., R.L. Naff and D.W. Hubbell, Temporal variations in beload transport rates associated with the migration of bedforms, *Earth Surf. Proc. Land.*, *14*, 135-156, 1989.

Gomez, B., and J.D. Phillips, Deterministic uncertainty in bed load transport, *J. Hydraul. Eng., 125*, 305-308, 1999.

Hersen, P., On the crescentic shape of barchan dunes, *Euro. Phys. J. B*, *37*, 507-514, 2004.

Hino, M., Equilibrium-range spectra of sand waves formed by flowing water, *J. Fluid. Mech.*, *34*, 565-573, 1968.

Howard, A.D., A detachment-limited model of drainage basin evolution, *Water Resour. Res.*, *30*, 2261-2285, 1994.

Jain, S.C., and J.F. Kennedy, The spectral evolution of sedimentary bed forms, *J. Fluid Mech.*, *63*, 301-314, 1974.

Jerolmack, D.J., and D. Mohrig, Frozen dynamics of migrating bedforms, *Geology*, *33*, 57-60, 2005.

Leclair, S.F., Preservation of cross-strata due to the migration of subaqueous dunes: An experimental investigation, *Sedimentology, 49*, 1157-1180, 2002.

Levey, R.A., B. Kjerfve, and R.T. Getzen, Comparison of bed form variance spectra within a meander bend during flood and average discharge, *J. Sed. Petr.*, *50*, 149-155, 1980.

Maddux, T. B., J. M. Nelson, and S. R. McLean, Turbulent flow over three-dimensional dunes: 1. Free surface and flow response, *J. Geophys. Res.*, *108*, 6009, doi:10.1029/2003JF000017, 2003.

Maddux, T. B., S. R. McLean, and J. M. Nelson, Turbulent flow over three-dimensional dunes: 2. Fluid and bed stresses, *J. Geophys. Res.*, *108*, 6010, doi:10.1029/2003JF000018, 2003.

McLean, S.R., The stability of ripples and dunes, *Earth-Sci. Rev.*, *29*, 141-144, 1990.

McLean, S.R., J.M. Nelson and S.R. Wolfe, Turbulence structure over two-dimensional bed forms: Implications for sediment transport, *J. Geophys. Res., 99*, 12729-12747, 1994.

Meyer-Peter, E., and R. Müller, Formulas for bed-load transport, *Int. Assoc. Hydraul. Res.*, *2nd Meeting*, Stockholm, pp.39-64, 1948.

Mohrig, D., Spatial evolution of dunes in a sandy river, Ph. D. dissertation, 119 pp., Univ. of Wash., Seattle, 1994.

Mohrig, D and J.D. Smith, Predicting migration rates of subaqueous dunes, *Water Resour. Res., 32*, 3207-3217, 1996.

Murray, A.B., and C. Paola, Properties of a cellular braided-stream model, *Earth Surf. Proc. Land.*, *22*, 1001-1025, 1997.

Nelson, J.M., S.R. McLean, and S.R. Wolfe, Mean flow and turbulence fields over two-dimensional bed forms, *Water Resour. Res.*, *29*, 3935–3953, 1993.

Nelson, J.M, R.L. Shreve, S.R. McLean and T.G. Drake, Role of near-bed turbulence structure in bed load transport and bed form mechanics, *Water Resour. Res., 31*, 2071-2086, 1995.

Nikora, V.I., and D.M. Hicks, Scaling relationships for sand wave development in unidirectional flows, *J. Hydraul. Eng., 123*, 1152-1156, 1997.

Nikora, V.I., A.N. Sukhodolov, and P.M. Rowinski, Statistical sand wave dynamics in one-directional water flows, *J. Fluid Mech.*, *351*, 17-39, 1997.

Niño, Y., A. Atala, M. Barahona and D. Aracena, Discrete particle model for analyzing bedform development, *J. Hydraul. Eng., 128*, 381-389, 2002.

Nordin, C.F., Statistical properties of dune profiles, *U.S. Geol. Survey*, *Prof. Paper* 562-F, 1971.

Parker, G., Lateral bed load transport on side slopes, *J. Hydraul. Eng.*, *110*, 197-199, 1984.

Pelletier, J.D., Self-organization and scaling relationships of evolving river networks, *J. Geophys. Res.*, *104*, 7359-7375, 1999.

Press, W.H., S.A. Teukolsky, W.T. Vetterling, and B.P. Flannery, Numerical Recipes in C, Cambidge U. Press, Cambridge, 1988.

Prigozhin, L., Nonlinear dynamics of Aeolian sand ripples, *Phys. Rev. E*, *60*, 729-733, 1999.

Rubin, D.M, Use of forecasting signatures to help distinguish periodicity, randomness, and chaos in ripples and other spatial patterns, *Chaos*, *2*, 525-535, 1992.

Schmeeckle, M.W., and J.M. Nelson, Direct simulation of bedload transport using a local, dynamic boundary condition, *Sedimentology, 50*, 279-301, 2003.

Schwämmle, V., and H. Herrmann, Modelling transverse dunes, *Earth Surf. Proc. Land.*, *29*, 769-784, 2004.

Shimizu, Y., M.W. Schmeeckle, and J.M. Nelson, Three-dimensional calculation of flow over two-dimensional dunes, *Japan Soc. Civil Eng. Ann. J. Hydraul. Eng*, *43*, 623-628, 2000.

Smith, J.D., Stability of a sand bed subjected to a shear flow of low Froude number, *J. Geophys. Res.*, *75*, 5928-5940, 1970.

Soo, S.L., Ed., Instrumentation for Fluid-Particle Flow. *William Andrew Publishing*, 412 pp., 1999.

Sumer, B.M., L.H.C. Chua, N.-S. Cheng, and J. Fredsøe, Influence of turbulence on bed load sediment transport, *J. Hydraul. Eng., 129*, 585-596, 2003.

Terzidis, O., P. Claudin and J.P. Bouchaud, A model for ripple instabilities in granular media, *Euro. Phys. J. B, 5,* 245-249, 1998.

Tufillaro, N.B., Discrete dynamical models showing pattern formation in subaqueous bedforms, *Int. J. Bifurcations Chaos*, *3*, 779-784, 1993.

Valance, A., and F. Rioual, A nonlinear model for aeolian sand ripples. *Euro. Phys. J. B*, *10*, 543-548, 1999.

van den Berg, J.H., Bedform migration and bed-load transport in some rivers and tidal environments, *Sedimentology, 34*, 681-698, 1987.

Werner, B.T., Eolian dunes: Computer simulations and attractor interpretation, *Geology*, *23*, 1107-1110, 1995.

Werner, B.T., Complexity in natural landform patterns, *Science*, *284*, 102-104, 1999.

Werner, B.T, and G. Kocurek, Bed-form dynamics: does the tail wag the dog?, *Geology*, *25*, 771-774, 1997.

Werner, B.T, and G. Kocurek, Bedform spacing from defect dynamics, *Geology*, *27*, 727-730, 1999.

Wiberg, P. L., and J. D. Smith, Model for calculating bed load transport of sediment, *J. Hydraul. Eng., 115,* 101-123, 1989.

Willgoose, G., R.L. Bras, and I. Rodriguez-Iturbe, A coupled channel network growth and hillslope evolution model: 1. Theory, *Water Resour. Res.*, *27*, 1671-1684, 1991.

Yizhaq, H., N.J. Balmforth, and A. Provenzale, Blown by wind: nonlinear dynamics of aeolian sand ripples, *Physica D*, 207-228, 2004.

Figure Captions

Figure 1. North Loup River topography extracted from images. Flow is from left to right for this and all figures. (a) Plan view snapshot in time of channel bottom, where brighness corresponds to water depth. Dashed line represents location of profiles in (b) and (c). (b) Sequential stream-bed profiles, shown every 120 s with vertical offset to allow visualization. (c) Space-time plot of sequential stream-bed profiles shown every 60 s, with elevation represented by brightness. Bedform crests and troughs are light and dark, respectively. Color scale same as (a).

Figure 2. Example of North Loup River spatial scaling of roughness for 20 downstream profiles, averaged at a snapshot in time. Interface width grows as a power law in the scaling regime, with the slope equal to the roughness exponent, α; equation is a best-fit linear regression to log-log data. Growth rolls over at the transition length, l_x, with corresponding roughess value, w_x . Error bars represent one standard deviation.

Figure 3. Definition sketch of the model shown in oblique perspective, with coordinate axes displayed. The mean elevation of the sediment-fluid interface (channel bottom) is shown by the dashed line, which is defined as $\eta = 0$ and used as the datum for mean water depth, $\langle h \rangle$. Elevations above and below this line are positive and negative, respectively.

Figure 4. Deterministic model (run D, table 1) evolution. (a) Oblique view snapshot of transient evolution of bed surface, at time = $1500\Delta t$. (b) Profile down the centerline of the 2D model domain, showing growth of bedforms from a flat surface. Compare to figure 4 of *Coleman and Melville* [1996]. Profiles are plotted every $20\Delta t$ from zero up to time $=1500\Delta t$.

Figure 5. Growth of roughness in time from a flat surface, calculated from averaging all downstream profiles at each time step, for (a) deterministic, and (b) noisy simulations. Dotted line is the exponential growth relation (18) in the text with $\gamma = 6$, while dashed line is the power law growth relation (19) with $\beta = 0.28$. Interface width and time are scaled by their respective equilibrium values; see text for details. Relations (18) and (19) were derived from flume studies, and were not fit to model data.

Figure 6. Stochastic model topography (run S, table 1) where roughness is in statistical steady state – compare to Fig. 1. (a) Plan view snapshot. (b) sequential profiles shown every $1500\Delta t$. (c) Space-time plot of sequential profiles shown every time step.

Figure 7. Example of spatial scaling of roughness for stochastic model (run S) and North Loup River at statistical steady state using a downstream profile at a snapshot in time; w and l are normalized by their transition values. See caption of Fig. 2 for explanation – note linear scale. Inset is the same data plotted on a log-log scale. No calibration was performed to match model with river data.

Table 1. Model parameters used for all runs – see equations 13-17.

Parameter	D	S
Δx	0.1	0.2
Δt	0.005	0.002
A	4.3	4.3
B	4.3	4.3
D	0.025	0.025
E	1	1
ζ	0	0.1(*randn*)
τ_b	0.07	0.07
$\langle h \rangle$	1	1
m	1	1
n	1.5	1.5
θ_c [°]	34	34
p	0.4	0.4

Boundary conditions are periodic in the downstream (x) direction and zero flux in the cross-stream (y) direction; the noise term $\zeta = 0.1$(*randn*), where *randn* represents a random variable having a normal distribution with zero mean and variance of one. *D* and *S* refer to model runs where *D* means deterministic and *S* means stochastic. Units are arbitrary unless specified.

Figure 1

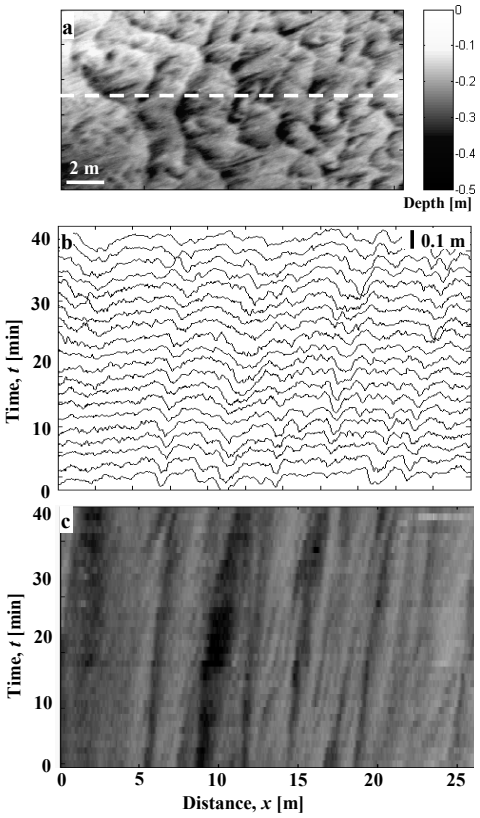
a
2 m
0
-0.1
-0.2
-0.3
-0.4
-0.5
Depth [m]
b
0.1 m
Time, t [min]
40
30
20
10
0
c
Time, t [min]
0
5
10
15
20
25
Distance, x [m]

Figure 2

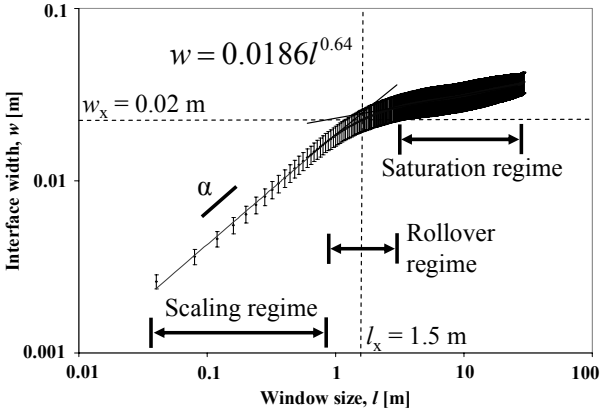
0.1
0.01
0.001
$w = 0.0186l^{0.64}$
w_x = 0.02 m
α
Saturation regime
Rollover
regime
Scaling regime
l_x = 1.5 m
Interface width, w [m]
0.01
0.1
1
10
100
Window size, l [m]

Figure 3

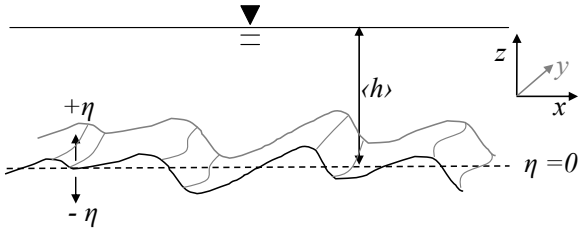

Figure 4

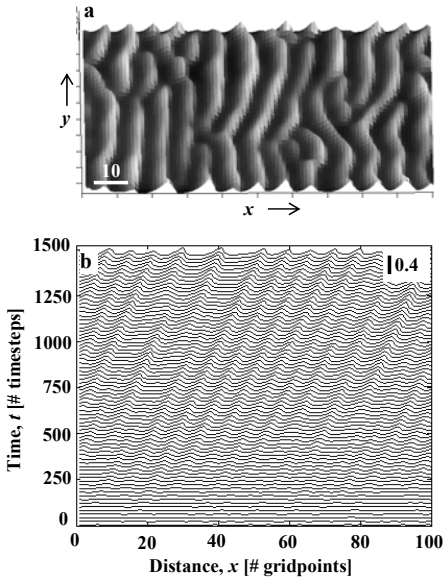
a
y
10
x
b
0.4
1500
1250
1000
750
500
250
0
Time, t [# timesteps]
0
20
40
60
80
100
Distance, x [# gridpoints]

Figure 5

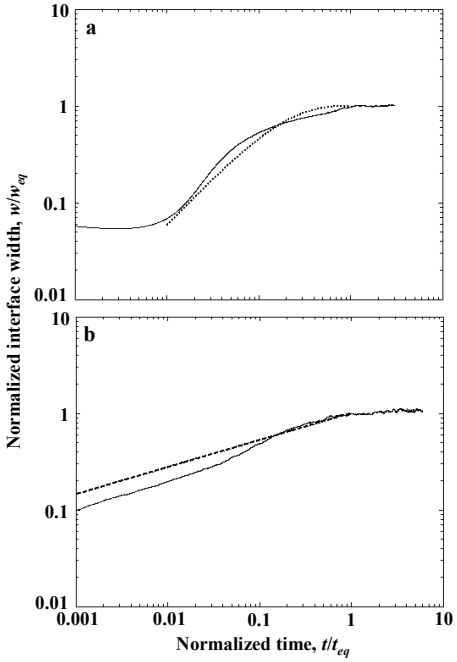
a
b
10
1
0.1
0.01
0.001
0.01
0.1
1
10
Normalized interface width, w/w_{eq}
Normalized time, t/t_{eq}

Figure 6

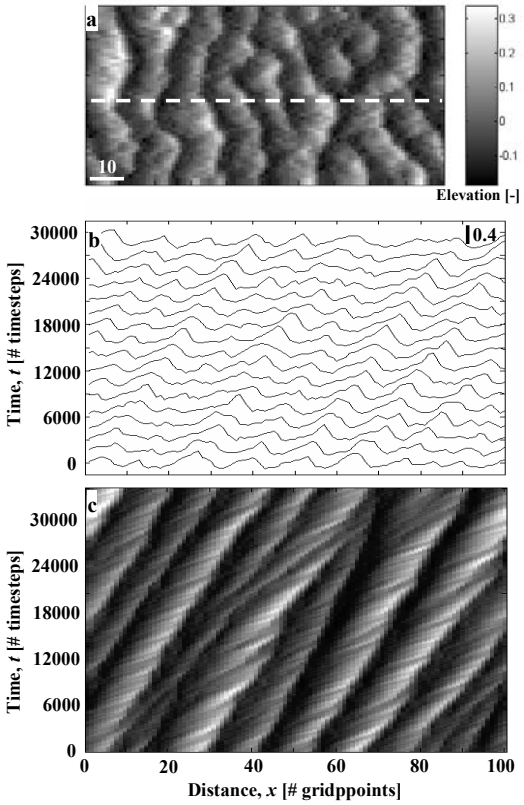
a
10
0.3
0.2
0.1
0
-0.1
Elevation [-]
b
0.4
30000
24000
18000
12000
6000
0
Time, t [# timesteps]
c
30000
24000
18000
12000
6000
0
Time, t [# timesteps]
0
20
40
60
80
100
Distance, x [# gridppoints]

Figure 7

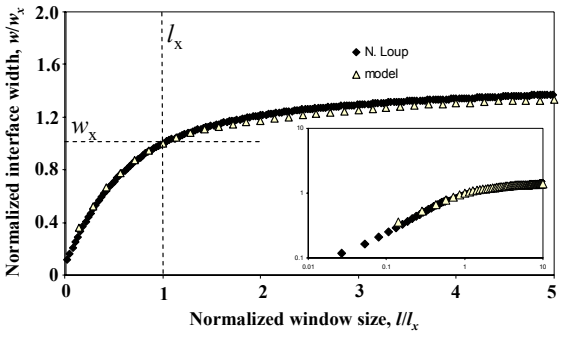
Normalized interface width, w/w_x
Normalized window size, l/l_x
l_x
w_x
N. Loup
model
2.0
1.6
1.2
0.8
0.4
0
0
1
2
3
4
5